






# Simple methods to test the accuracy of MRgFUS robotic systems

Anastasia Antoniou<sup>1</sup> | Theocharis Drakos<sup>2</sup> | Marinos Giannakou<sup>2</sup>  |  
Nikolas Evripidou<sup>1</sup>  | Leonidas Georgiou<sup>3</sup> | Theodora Christodoulou<sup>3</sup> |  
Natalie Panayiotou<sup>3</sup> | Cleanthis Ioannides<sup>3</sup> | Nikolaos Zamboglou<sup>3</sup> |  
Christakis Damianou<sup>1</sup> 

<sup>1</sup>Department of Electrical Engineering, Computer Engineering, and Informatics, Cyprus University of Technology, Limassol, Cyprus

<sup>2</sup>R&D, Medsonic LTD, Limassol, Cyprus

<sup>3</sup>German Oncology Center, Limassol, Cyprus

## Correspondence

Christakis Damianou, Department of Electrical Engineering, Computer Engineering, and Informatics, Cyprus University of Technology, 30 Archbishop Kyprianou St, Limassol 3036, Cyprus.  
Email: [christakis.damianou@cut.ac.cy](mailto:christakis.damianou@cut.ac.cy)

## Funding information

Research and Innovation Foundation of Cyprus, Grant/Award Numbers: ENTERPRISES/0618/0016, ENTERPRISES/0918/0012, INTEGRATED/0918/0008

## Abstract

**Background:** Robotic-assisted diagnostic and therapeutic modalities require a highly accurate performance to be certified for clinical application. In this paper, three simple methods for assessing the accuracy of motion of magnetic resonance-guided focused ultrasound (MRgFUS) robotic systems are presented.

**Methods:** The accuracy of motion of a 4 degrees of freedom robotic system intended for preclinical use of MRgFUS was evaluated by calliper-based and magnetic resonance imaging (MRI) methods, as well as visually by performing multiple ablations on a plastic film.

**Results:** The benchtop results confirmed a highly accurate motion in all axes of operation. The spatial positioning errors estimated by MRI evaluation were defined by the size of the imaging pixels. Lesions arrangement in discrete and overlapping patterns confirmed satisfactory alignment of motion trajectories.

**Conclusions:** We believe the methods presented here should serve as a standard for evaluating the accuracy of motion of MRgFUS robotic systems.

## KEYWORDS

motion accuracy, MRgFUS robotic devices, simple evaluation methods

## 1 | INTRODUCTION

The introduction of robots in medicine has been essential for establishing minimally invasive diagnostic and therapeutic modalities by extending their benefits to most surgical specialties.<sup>1</sup> Robotic devices are continuously being invented to aid in the positioning and manipulation of surgical instruments and energy sources. Such robotic-assisted procedures require a highly accurate operation to approach a target in a minimally invasive manner and meet the clinical requirement. Simultaneously, the

accuracy data are essential for establishing safety guidelines for clinical applications.

All the techniques used to test the mechanical accuracy of a robot are based on the idea of comparing the commanded motion step with the actual displacement as estimated by a distance-measuring technique. Mechanical accuracy refers to both the positioning and repeatability accuracy of motion. Before the procedure is applied and evaluated in vivo, accuracy assessment is typically carried out in free space, sometimes referred to as intrinsic system accuracy, meaning not under real conditions. Most commonly, after acquiring evidence of

This is an open access article under the terms of the Creative Commons Attribution-NonCommercial License, which permits use, distribution and reproduction in any medium, provided the original work is properly cited and is not used for commercial purposes.

© 2021 The Authors. The International Journal of Medical Robotics and Computer Assisted Surgery published by John Wiley & Sons Ltd.



sufficient accuracy and repeatability by benchtop testing, the system is evaluated in the environment that is intended to be clinically used, such as the bore of a magnetic resonance imaging (MRI) system. This is essential for ensuring that the system maintains a high degree of accuracy in real-like scenarios. Even a minimal magnetic shift of the system's components in the MRI could affect the accuracy and compromise the patient's safety in highly sensitive procedures.

Regarding benchtop evaluation, several motion-tracking techniques were proposed for assessing the accuracy of motion in a free robot workspace.<sup>2-7</sup> Optical tracking systems have been widely used for confirming adequate targeting accuracy for needle-related interventions, where the placement error is defined by the deviation of the actual tooltip position from the desired location.<sup>2-5</sup> The accuracy of an automated robot intended for breast biopsy in precisely reaching a target was evaluated using a rigid test tool, which was driven to target positions through straight and angled paths and monitored with an optical tracker.<sup>2</sup> Similarly, Patriciu et al.<sup>3</sup> investigated the motion accuracy of a system for automated brachytherapy seed placement using an optical tracking system. An active marker was mounted on the end-effector of the robotic arm allowing continuous tracking of its position. An optical tracking system was also used by Patel et al.<sup>4</sup> who evaluated a robotic system intended to perform shoulder arthrography. A specially designed frame with optical markers served as the reference, while a tracking structure was also integrated on the needle guide so that its position can be tracked relative to the reference frame.<sup>4</sup> A different tracking method was chosen by Dou et al.<sup>5</sup> who measured the positioning accuracy of a brachytherapy system using a 3D laser tracker, as well as an inertial measurement unit.<sup>5</sup> An optical measuring microscope has also been proposed for estimating the actual displacement of a linear motion stage after the execution of commanded movements of varying distance.<sup>6</sup> In another study,<sup>7</sup> the displacement of an endoscope manipulator was measured with two charge-coupled device laser micrometres.

More straightforward methods involving the use of digital callipers and special structures have also been carried out in the laboratory environment for accuracy evaluation purposes. The needle tip accuracy of a breast biopsy robot was evaluated in free air by targeting crosshairs drawn on a board.<sup>8</sup> The needle tip was commanded to puncture these targets, and the error was estimated by the distance from the centre of each target to the corresponding pierced hole.<sup>8</sup> Similarly, in the framework of evaluating the motion accuracy of a robot intended for transcranial focussed ultrasound (FUS) surgery, the FUS transducer was replaced by a felt-tipped pen, which was commanded to touch multiple resolution points distributed on three perpendicular planes demonstrating the entire robot's workspace.<sup>9</sup> Each created mark was assigned in resolution circles having radial and angular approximation zones for facilitating targeting error measurement.<sup>9</sup> Another simplified method involves mounting digital callipers on the motion stages of a robot such that their actual displacement after motion execution can be directly measured by the incremental distance of the calliper.<sup>10,11</sup>

After assessing the accuracy of needle-related interventions in free space, experiments under more realistic conditions are typically

performed. Initial experiments are predominantly performed in phantoms in an imaging environment, involving the use of fiducial markers for visualizing and registering the system in the imaging coordinates. A first planning scan is typically acquired for selecting the target locations in the phantom and calculating the insertion parameters.<sup>12-14</sup> Following targeting according to the estimated coordinates exported to a motor controller software, confirmation images are collected for assessing the accuracy of needle placement relative to the prescribed locations.<sup>12-14</sup> In a phantom study performed by Patel et al.<sup>12</sup> under real-time MRI guidance, a needle-based therapeutic ultrasound applicator was robotically inserted in a gelatine phantom in locations predefined in 3D slicer. The intended probe tip position was compared to the actual position as visualized in 3D-fast field echo images. Likewise, Krieger et al.<sup>13</sup> assessed the accuracy of motion of a system for prostate interventions in a tissue-mimicking phantom. The rectal sheath was automatically aligned with the desired insertion point and then manually inserted in the phantom. The void caused by the needle tip was visualized in axial turbo spin echo proton density images enabling calculation of the in-plane error of targeting.<sup>13</sup> Targeting accuracy assessment in MRI was also performed in air with the use of a gadolinium filled virtual needle, which was tracked and visualized using T1-weighted Isotropic Volume Examination sequence.<sup>14</sup>

Robotic devices intended for non-invasive FUS applications are constantly being developed<sup>15</sup> and extensively evaluated by performing ablation studies, in which the separation precision of multiple ablations constitutes an indication of the positioning error. Tao Wu et al.<sup>16</sup> performed quality control of a FUS system, where the focus positioning accuracy was tested by performing multiple sonications on a Lucite cart. The transducer was accommodated in a water tank to be acoustically coupled to the target. Left-right and superior-inferior movements by specific distance were commanded by a treatment planning software, resulting in numerous sets of melted spots arranged in discrete patterns. The actual distance between adjacent spots was measured with a digital calliper.<sup>16</sup> In other phantom experiments conducted in a benchtop setting,<sup>10</sup> the linear motion stages were commanded to create discrete ablations of specific spacing in a gel phantom. White coagulation lesions were clearly visible, being spaced by the desired step, thus confirming the accuracy of positioning.

Price et al.<sup>9</sup> followed a similar approach but in an MRI setting. An MR conditional robot for transcranial FUS interventions was used to perform multiple sonications in a  $2 \times 3$  pattern in a heat-sensitive gel phantom located in a water tank. The thermal images acquired after each sonication were superimposed onto one image, and the positioning accuracy was defined as the spacing between the centres of adjacent ablated areas.<sup>9</sup> This technique was also selected for evaluating the accuracy of motion of an MR-compatible FUS device intended for brain diseases treatment.<sup>17</sup> A four-point ablation pattern was performed in vitro, in lamb brain, with different motion steps of 1–10 mm, and the formed lesions were visualized in T1-weighted fast spin echo (FSE) images. The ablated areas appeared as spots of increased signal intensity, and the distance between neighbouring ablations was calculated from the centre of each spot. Notably, smaller errors were estimated with increasing step

distance.<sup>17</sup> Similarly, Yiallouras et al.<sup>11</sup> performed phantom experiments where T2-weighted FSE images revealed areas of reduced signal formed in a discrete pattern. It is notable that Sagias et al.<sup>18</sup> developed a motion phantom for evaluating FUS protocols specifically for moving targets in the MRI environment. In another study carried out in a gel phantom,<sup>19</sup> the robotic arm of an US-guided FUS ablation system was commanded to move the focal point to ablate the four corners of the phantom, and the targeting accuracy was assessed by visualizing the sonicated areas on US images.

Herein, we present three simple methods that were used for assessing the accuracy of motion of a magnetic resonance-guided focused ultrasound (MRgFUS) robotic system in both benchtop and MRI environments. The system is intended for ex vivo and in vivo preclinical use, including studies in companion animals of all sizes with naturally occurring tumours. In the first method, a digital calliper is mounted on the motion stage under evaluation with the assistance of specially designed 3D-printed parts, having its one edge fixed on a stationary part and the other on a movable part. In that way, a specific step movement of the stage results in an analogous increment in the calliper. The second evaluation procedure relates to accuracy assessment in the MRI setting. The robotic device is sited on the MRI couch, and a plastic marker is mounted on the top of the FUS transducer so that it can be visualized in MR images. The third method involves performing multiple ablations in a transparent plastic film by robotic movement of the transducer.

## 2 | MATERIALS AND METHODS

### 2.1 | Robotic system

A robotic system featuring 4 degrees of freedom (DOF) was developed to be used in the preclinical setting for ex vivo and in vivo applications of the MRgFUS technology. It is particularly intended to treat cancer in small and large companion animals with naturally occurring tumours.

The positioning device was designed (Inventor Professional 2018; Autodesk) and 3D-printed (F270; Stratasys Ltd.) with acrylonitrile butadiene styrene thermoplastic material. Some of the design

criteria included reduction of the total size of the device as much as possible while maintaining sufficient motion range. This compact design allows for easy incorporation of the device in the table of any conventional MRI scanner. A specially designed mattress is adapted around the protruding part of the device to raise the table to the exact height of the device.

The positioning mechanism features motion in 4 DOF, which is adequate to ablate a tissue volume of any shape and size. Specifically, the device allows the user to linearly navigate the focussed transducer in three axes (X, Y and Z), whereas angular rotation about a single axis is also available. The X and Y motion stages allow movement in two orthogonal horizontal axes, while the Z stage provides motion in a vertical axis. Accordingly, the  $\Theta$  stage enables rotation of the transducer about its shaft. All motion stages are computer-controlled through a customized software. Due to the constrain of the MRI bore, there are some spatial limits, and therefore, motion restrictions. The maximum travel of the transducer is 60 mm in the X axis (forward and reverse), 75 mm in the Y axis (left and right) and 26 mm in the Z axis (up and down). The rotation limit is 90°: 45° clockwise (CW) and 45° counter-clockwise (CCW). Piezoelectric motors (USR60-S3; Shinsei Corporation) and dual digital encoders (US Digital Corporation) were incorporated in all motion stages, thus providing a highly accurate motion. More precisely, the system is characterized by a high resolution of 500 lines per inch for the linear strip and 2500 lines for a full rotation of the plastic disk. The computer-aided design (CAD) drawing of the fully assembled robotic device is shown in Figure 1.

### 2.2 | Digital callipers method

The motion accuracy of the positioning mechanism was evaluated using digital callipers with a measuring accuracy of 0.01 mm. The digital callipers (one for the linear stages and one for the angular stage) were mounted and stabilized on 3D-printed structures. The structures were easily attached to the robotic device, as illustrated in Figure 2. In that way, the calliper was perfectly aligned with the axis under evaluation, thus providing accurate distance estimation. The one edge of the calliper was securely mounted on a stationary part of

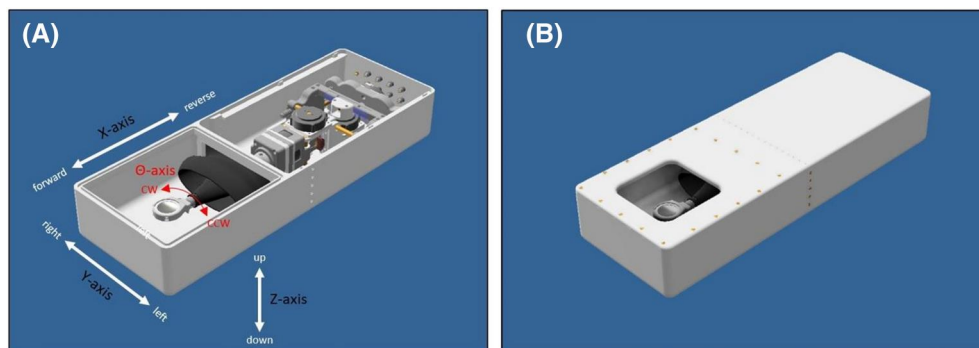
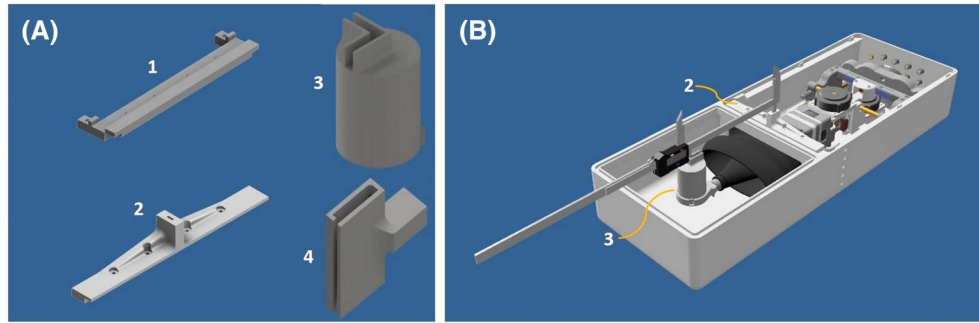


FIGURE 1 Computer-aided design drawing of the 4 degrees of freedom robotic system (A) without the cover (components are visualized) and (B) with the cover



**FIGURE 2** (A) Stationary (1, 2, 4) and moveable (3) 3D-printed structures that were used for the X and Y axes distance measurements and (B) computer-aided design drawing of the setup that was used for the X axis motion accuracy estimation

the device, while the other part was attached to the movable part (Figure 2). A different structure was used for the measurement of the angular motion, as shown in Figure 3. Note that this stage was evaluated separately, outside of the mechanism enclosure. In each case, the motion stage was moved through the designed software at a certain distance (or degrees), and the actual displacement was measured by the incremental distance in the calliper. Both directions of each linear axis were evaluated at step movements of 1, 5 and 10 mm. Accordingly, the angular motion accuracy was evaluated for CW and CCW directions at step angles of 1°, 5° and 10°.

Moreover, the speed of motion of the robotic device in all axes (X, Y, Z and  $\Theta$ ) and directions was calculated by the time required for the stage to cover specific step movements, which was equal to the activation time of the piezoelectric motors as provided by the software.

### 2.3 | MRI method

Another simple method for estimating the motion accuracy of a robotic system is through MRI. This method is limited to MR-compatible robotic devices. The concept of the proposed technique is based on the fact that structures without protons appear dark in MR images. The focused transducer was replaced by a 3D-printed plastic structure with a tip of 2 mm thickness, which served as a marker, and the water enclosure was filled with degassed water. The robotic device was placed inside an MRI scanner (1.5 T, GE Signa HD16; General Electric Healthcare) and covered with a Signa 1.5 T General Purpose flex surface coil (General Electric Medical Systems). Figure 4A illustrates the experimental setup as placed on the MRI table, while Figure 4B shows a CAD drawing of the plastic marker. MR scanning was performed using an FSE sequence in coronal plane. The main MRI parameters were: repetition time = 800 ms, echo time = 19 ms, flip angle = 90°, echo train length = 3, pixel bandwidth = 65.1 and field of view = 280 × 280 × 10 mm<sup>3</sup>.

The accuracy of linear motion was assessed in the X and Y axes. The initial position of the tip was located, and then the transducer was moved by a certain distance. Bidirectional movements with a step of 3 and 5 mm in both axes were tested. An MR image was

acquired after each step movement to detect the tip location. A special approach was followed for locating the position of the 2 mm thick tip of the plastic marker. First, the image zoom was enhanced to focus on the plastic marker. Then, the corresponding pixels were scanned to identify the x and y coordinates of the pixel with the lowest signal intensity (this was assumed to be the centre of the marker in the image). The change in pixel number after a step movement reflected the shift in position of the transducer in the tested direction. The pixel difference was then multiplied by the pixel size (0.5469 mm) of the acquisition matrix so as to measure the shift in millimetres. This technique had an inherent error of  $\pm 1$  pixel, which translated to  $\pm 0.5469$  mm. Finally, the series of images were superimposed onto one image for visualizing the motion patterns.

### 2.4 | Visual method

The motion accuracy was also assessed through visual observations of multiple ablations produced on a transparent plastic film (0.9 mm thickness, FDM400mc print plate; Stratasys Ltd.). The acoustic attenuation of the plastic film at the frequency of 2.1 MHz was  $8.5 \pm 0.2$  dB/cm-MHz based on a standard transmission through immersion technique.<sup>20</sup> The water enclosure containing the transducer (spherically focused, frequency: 1.1 MHz, diameter: 50 mm, focal length: 70 mm; Medsonic Ltd.) was filled with degassed water up to the plastic film. The robotic device was moved to sonicate the film in square grid patterns for evaluating the accuracy of motion, as well as the linear motion alignment in the X and Y axes. An acoustic power of 10 W was applied at each grid point using an RF amplifier (AG1012; T & C Power Conversion, Inc.). The sonication time varied from 1–4 s so as to control the lesion size. Subsequently, sonications were performed with varying motion step and sonication time, with the time delay between the successive sonications set at 30 s. Also, the maximum motion range of the positioning mechanism in the horizontal plane was estimated by applying sonications at the extreme points of movement in the X and Y axes. It is noted that lesion formation was a result of reflection from the plastic/air interface.

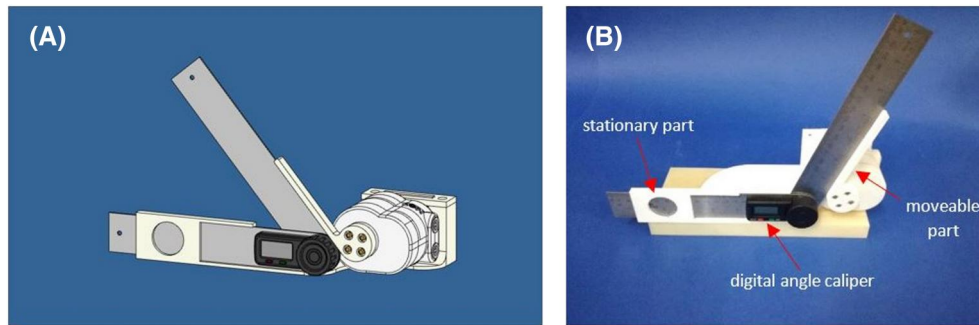


**FIGURE 3** Experimental setup used for estimating the angular motion accuracy using the digital angle caliper; (A) computer-aided design drawing and (B) photo

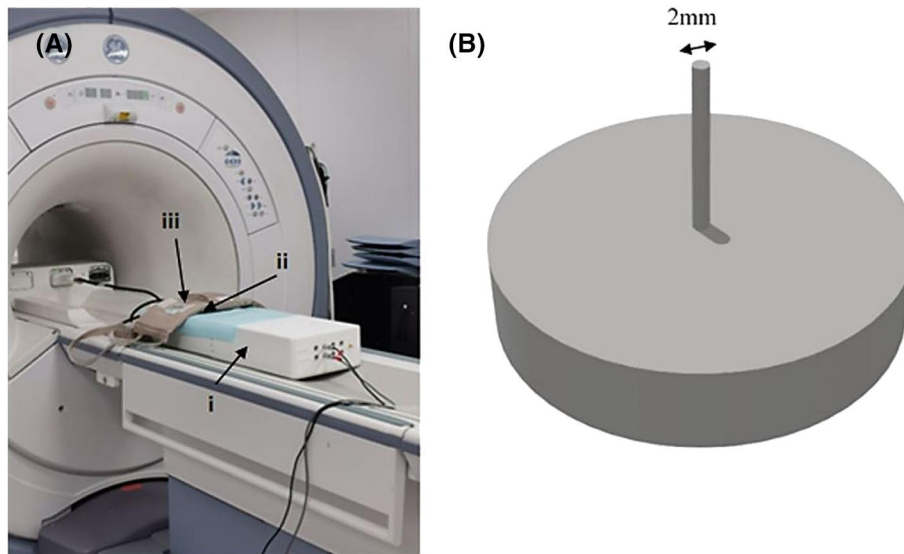


**FIGURE 4** (A) The robotic device (i) as placed on the magnetic resonance imaging table, showing the location of the plastic marker (ii) and the flex surface coil (iii), and (B) computer-aided design drawing of the plastic marker used for accuracy measurements

### 3 | RESULTS

The motion accuracy of the robotic device in both linear and angular axes was evaluated using digital callipers. Linear motion steps of 1, 5 and 10 mm and angular steps of 1°, 5° and 10° were performed for 20 repetitions in bidirectional movements. Figure 5 shows a bar chart that displays the actual distance measured at a commanded step movement of 5 mm in both  $X$  axis directions for each repetition measurement. The range of actual displacement measured at each commanded step, as well as the mean motion error and standard deviation for all the axes ( $X$ ,  $Y$ ,  $Z$  and  $\Theta$ ) are listed in Table 1. Furthermore, the speed of motion of all stages in bidirectional movements was calculated according to the motors' activation time during movement execution. The corresponding results are also listed in Table 1.

MRI was also used to examine the accuracy of motion in the  $X$  and  $Y$  axes. The MR images acquired after execution of each 3 mm motion step in the  $X$  axis reverse and  $Y$  axis right directions were superimposed onto the images shown in Figure 6A,B, respectively. Table 2 lists the range of actual distance measured for each

commanded motion step (3 and 5 mm) and each direction, as well as the corresponding mean motion error and standard deviation.

The motion accuracy was visually observed by sonicating plastic films. Sonications at the extreme points of movement in the horizontal plane revealed a maximum motion range equal to 6 and 7 cm in the  $X$  and  $Y$  axes, respectively. The effect of lesion formation on the plastic film was originally examined by varying the sonication time while keeping constant the acoustic power as shown in Figure 7. The appropriate selection of sonication time and grid step allowed formation of discrete and overlapping lesions and visual evaluation of the accuracy of motion and alignment. Figure 8 shows discrete lesions formed after applying sonications at acoustical power of 10 W for 1 s, in a  $6 \times 5$  grid pattern with a step distance of 5 mm. The formed lesions show satisfactory alignment in both axes. Sonications at the same acoustical power for a longer time of 3 s in a  $15 \times 15$  grid pattern with the same time delay of 30 s, but a smaller spatial step of 2 mm, resulted in overlapping lesions as illustrated in Figure 9. The ablated area was well defined in a square of about  $3.3 \times 3.3$  cm<sup>2</sup>, without any significant protrusions.

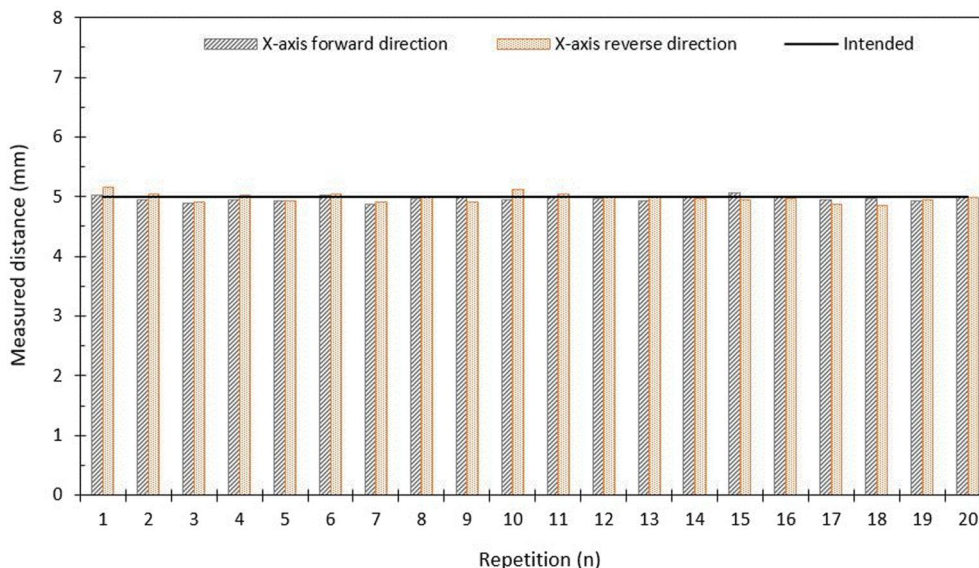


**FIGURE 5** Distance measurements for 20 repetitions in the X-axis with step movement of 5 mm in bidirectional movements. The black straight line indicates the commanded distance

## 4 | DISCUSSION

In this paper, three simple and practical methods for assessing the accuracy of motion of a robotic device are described. It is emphasized that the calliper and MRI methods are suitable for evaluating any robotic system, while ablation of the plastic film is intended specifically for FUS systems. It is also noted that the device should be MR-compatible in order to be properly evaluated in an MRI environment. All these methods are based on the idea of evaluating the performance of the device in accurately executing commanded movements.

First, the motion accuracy of an MRgFUS robotic device was evaluated using digital callipers integrated on the motion stages under evaluation using specially designed 3D-printed structures. The mean error of linear motion varied from  $0.042 \pm 0.032$  mm for the 1 mm step in the X axis forward direction to  $0.123 \pm 0.082$  mm for the 10 mm step in the Y axis right direction. Accordingly, the mean error of angular motion varied from a minimum value of  $0.100 \pm 0.077^\circ$  for the  $1^\circ$  step to a maximum value of  $0.320 \pm 0.225^\circ$  for the  $10^\circ$  step (CW rotation). Contrary to the findings of a previous study,<sup>17</sup> the mean error was found to be increasing with increasing motion step for all four axes.

The speed of motion was estimated by the time activation of the robot's motors as provided by the controlling software during motion execution. The results revealed no significant difference in speed of motion for bidirectional movements. A mean motion speed of approximately 10 mm/s was estimated for both the X and Z axes, while a higher value of about 14 mm/s was found for the Y axis.

In comparison with previous designs,<sup>10,11,17,21</sup> the principle of movement of the proposed one was significantly improved by the dual encoder positioning control that guarantees a smooth, reliable and highly accurate motion in all stages. Additionally, the problem of

reduced accuracy for small steps previously observed<sup>17</sup> seems to be solved by using faster software commands that makes the encoder's reading more accurate.

The system was then evaluated in the MRI environment that is intended to be used. The accuracy of motion remains satisfactory during full operation of the system in the MRI environment. Additionally, there was no evidence of any magnetically induced shift of the mechanical components that could compromise the accuracy of ultrasound delivery to the target, and therefore the patient's safety.

The spatial positioning errors estimated by the benchtop setting using digital callipers are significantly smaller than those obtained in the MRI setting. This is attributed to the size of voxels of the MR images that determine the finest possible accuracy. Given the MRI resolution of about 0.55 mm per pixel, the estimated motion errors are within a reasonable range. Although this approach suffers from imaging resolution limitations, a smaller pixel could provide more precise distance estimates, but at the cost of increased image acquisition time and reduced signal to noise ratio.

The high degree of accuracy evidenced by benchtop testing with callipers was also confirmed by multiple ablations on a transparent plastic film. The melted spots formed after grid ablation were arranged in a discrete pattern, in a highly accurate manner, clearly demonstrating that the linear stages were moved by the commanded step. As observed, the centres of almost all the spots were equally spaced, demonstrating excellent repeatability. Multiple ablations in a grid with a smaller spatial step between adjacent sonications and three times longer sonication time resulted in a well-defined square area of overlapping lesion. The results suggest that the system can precisely ablate a large tissue volume by overlapping lesions.

The aforementioned ablation method is intended specifically for testing the accuracy of FUS systems and is essential for assessing

**TABLE 1** The range of distance measurements as estimated by the digital callipers at commanded spatial steps of 1, 5 and 10 mm in each linear axis and angular step of 1°, 5°, and 10° about the rotational axis, the corresponding mean motion error and standard deviation and the mean speed and standard deviation in each case

Linear axis	Commanded step (mm)	Range of actual displacement (mm)	Mean error ± SD forward (mm)	Mean error ± SD reverse (mm)	Mean speed ± SD forward (mm/s)	Mean speed ± SD reverse (mm/s)
X	1	0.88–1.08	0.042 ± 0.032	0.051 ± 0.032	10.31 ± 0.62	10.05 ± 0.26
	5	4.85–5.15	0.047 ± 0.033	0.065 ± 0.044	10.43 ± 0.57	9.80 ± 0.94
	10	9.78–10.19	0.081 ± 0.058	0.058 ± 0.057	10.01 ± 0.21	9.98 ± 0.78
Y	Commanded step (mm)	Range (mm)	Error right (mm)	Error left (mm)	Speed right (mm/s)	Speed left (mm/s)
	1	0.88–1.09	0.045 ± 0.042	0.042 ± 0.026	14.28 ± 1.40	15.93 ± 0.83
	5	4.89–5.19	0.053 ± 0.032	0.084 ± 0.050	13.84 ± 1.02	14.16 ± 0.62
Z	Commanded step (mm)	Range (mm)	Error up (mm)	Error down (mm)	Speed up (mm/s)	Speed down (mm/s)
	1	0.89–1.11	0.052 ± 0.029	0.039 ± 0.030	9.90 ± 0.20	10.09 ± 0.21
	5	4.90–5.11	0.055 ± 0.037	0.055 ± 0.035	9.90 ± 0.13	9.73 ± 0.30
Angular axis	Commanded step (°)	Range (°)	Error CW (°)	Error CCW (°)	Speed CW (°/s)	Speed CCW (°/s)
	1	0.8–1.3	0.100 ± 0.077	0.155 ± 0.097	132.4 ± 12.2	118.8 ± 16.2
	5	4.7–5.7	0.250 ± 0.175	0.245 ± 0.193	144.5 ± 10.8	145.1 ± 10.2
Angular axis	Commanded step (°)	Range (°)	Error CW (°)	Error CCW (°)	Speed CW (°/s)	Speed CCW (°/s)
	10	9.9–10.7	0.320 ± 0.225	0.290 ± 0.251	148.4 ± 3.74	144.5 ± 3.2

Abbreviations: CW, clockwise; CCW, counter-clockwise.

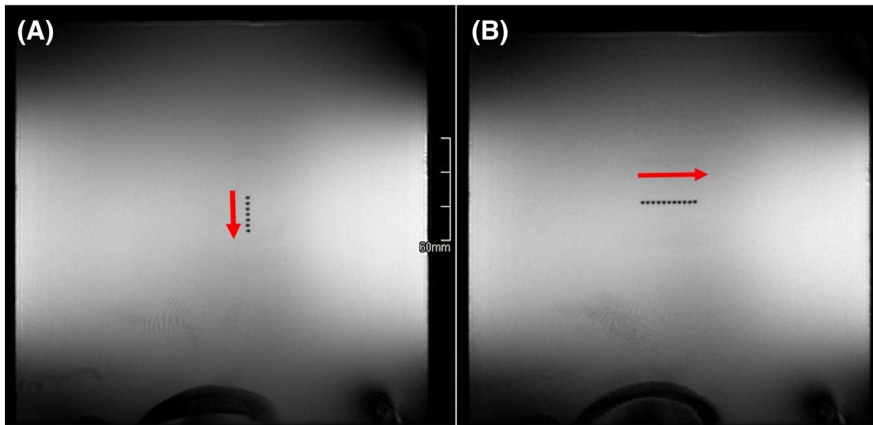


**FIGURE 6** Minimum intensity projection from a combination of fast spin echo coronal images that shows a (A) reverse step movement of 3 mm in the X direction and (B) right step movement of 3 mm in the Y direction

**TABLE 2** The range of distance measurements as estimated by MRI at commanded spatial steps of 3 and 5 mm in X and Y axes bidirectional movements, and the corresponding mean motion error and standard deviation

Linear axis	Commanded step (mm)	Range of actual displacement (mm)	Mean error $\pm$ SD forward (mm)	Mean error $\pm$ SD reverse (mm)
X	3	2.73–3.83	$0.277 \pm 0.007$	$0.342 \pm 0.172$
	5	4.92–5.47	$0.339 \pm 0.184$	$0.352 \pm 0.179$
	Commanded step (mm)	Range of actual displacement (mm)	Mean error $\pm$ SD right (mm)	Mean error $\pm$ SD left (mm)
Y	3	2.73–3.83	$0.330 \pm 0.166$	$0.278 \pm 0.007$
	5	4.37–5.47	$0.171 \pm 0.191$	$0.286 \pm 0.239$

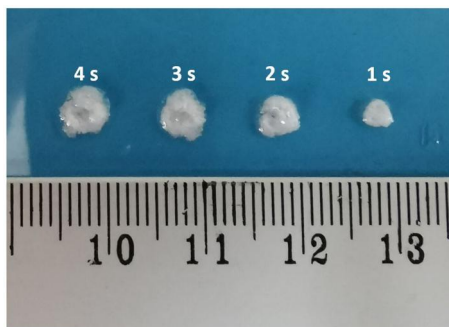


**FIGURE 7** Effect of varying sonication time on lesion formation on the plastic film, using low power and a spatial step of 10 mm (transducer specifications: 1.1 MHz frequency, 50 mm diameter and 70 mm focal length)

their ability to precisely deliver heating spots along the desired pattern. It is notable that in such systems, the accuracy in free robot workspace is representative of that in more realistic scenarios (phantom and in vivo experiments), whereas, for instance, in needle-based interventions is not. This is consistent with what has been previously reported by Price et al.,<sup>9</sup> who found that the intrinsic accuracy of a FUS system as estimated in the air was similar to that obtained by phantom experiments in the MRI setting.

The proposed methods were greatly improved in terms of accuracy compared to those we have previously used.<sup>10,11,22,23</sup> The

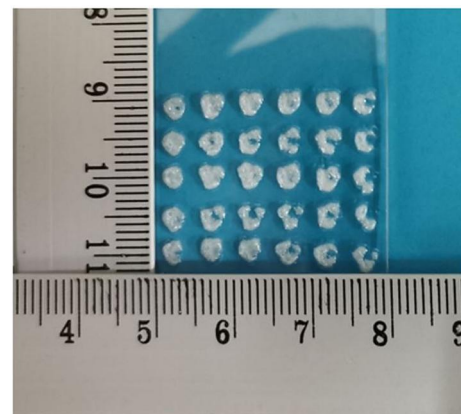


**FIGURE 8** Discrete lesions as formed on the plastic film for sonications in a  $6 \times 5$  grid pattern, with acoustical power of 10 W for 1 s and a step distance of 5 mm

quality of benchtop evaluation was enhanced by using 3D-printed structures specially designed for each individual axis, which provided perfect alignment of the calliper with each axis of measurement and reduced systematic errors.<sup>10</sup> Regarding the MRI evaluation, the accuracy of step movement has been previously estimated by locating the transducer on MR images.<sup>23</sup> Advantageously, a more accurate method is proposed herein, involving the use of a 2 mm plastic marker, which is clearly visible on MRI images using the appropriate sequence.



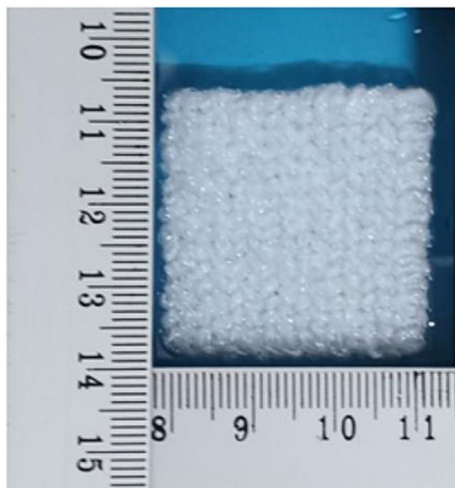


**FIGURE 9** Overlapping lesions as formed on the plastic film for sonications in a  $15 \times 15$  grid pattern, with acoustical power of 10 W for 3 s and a step distance of 2 mm

Overall, the accuracy of the tested robotic device, as proven from all three methods, is sufficient to guarantee an efficient performance of the system in terms of precise ablation in both laboratory and MRI environments. We believe the proposed methods should serve as the standard methods for evaluating FUS robotic systems.

#### ACKNOWLEDGEMENTS

The project was funded by the Research and Innovation Foundation of Cyprus under the projects: FUSROBOT (ENTERPRISES/0618/0016), PROSTASONIC (ENTERPRISES/0918/0012) and SOUNDPET (INTEGRATED/0918/0008).

#### CONFLICT OF INTERESTS

All declare no conflict of interest.

#### AUTHOR CONTRIBUTION

Anastasia Antoniou contributed in the drafting of the manuscript. Theocharis Drakos contributed in the benchtop evaluation of the motion accuracy of the robotic system and drafting of the manuscript. Marinos Giannakou contributed in the development of the robotic system. Nikolas Evripidou contributed in the development of the electronic system and 3D-printed structures. Leonidas Georgiou contributed in the MRI experiments. Theodora Christodoulou contributed in the MRI experiments. Natalie Panayiotou contributed in the MRI experiments. Cleanthis Ioannides contributed in the MRI experiments. Nikolaos Zamboglou contributed in the MRI experiments. Christakis Damianou served as the scientific coordinator and supervised the development of the system, implementation of the experiments and drafting of the manuscript.

#### DATA AVAILABILITY STATEMENT

The data that support the findings of this study are available from the corresponding author upon reasonable request.

#### ORCID

Marinos Giannakou  <https://orcid.org/0000-0002-6777-0515>

Nikolas Evripidou  <https://orcid.org/0000-0002-8200-3349>

Christakis Damianou  <https://orcid.org/0000-0003-0424-2851>

#### REFERENCES

- Peters BS, Armijo PR, Krause C, Choudhury SA, Oleynikov D. Review of emerging surgical robotic technology. *Surg Endosc*. 2018; 32(4):1636-1655. <https://doi.org/10.1007/s00464-018-6079-2>
- Chan KG, Fielding T, Anvari M. An image-guided automated robot for MRI breast biopsy. *Int J Med Robot Comput Assist Surg*. 2016;12(3):461-477. <https://doi.org/10.1002/rcs>
- Patriciu A, Petrisor D, Muntener M, Mazilu D, Schär M, Stoianovici D. Automatic brachytherapy seed placement under MRI guidance. *IEEE Trans Biomed Eng*. 2007;54(8):1499-1506. <https://doi.org/10.1109/TBME.2007.900816>
- Patel N, Yan J, Monfaredi R, Sharma K, Cleary K, Iordachita I. Pre-clinical evaluation of an integrated robotic system for magnetic resonance imaging guided shoulder arthrography. *Med Imaging*. 2019;6(2):1. <https://doi.org/10.1117/1.JMI.6.2.025006>
- Dou H, Jiang S, Yang Z, Sun L, Ma X, Huo B. Design and validation of a CT-guided robotic system for lung cancer brachytherapy. *Med Phys*. 2017;44(9):4828-4837. <https://doi.org/10.1002/mp.12435>
- Tavallaei MA, Johnson PM, Liu J, Drangova M. Design and evaluation of an MRI-compatible linear motion stage. *Med Phys*. 2016;43(1):62-71. <https://doi.org/10.1118/1.4937780>
- Koseki Y, Washio T, Chinzei K, Iseki H. Endoscope Manipulator for Trans-nasal Neurosurgery, Optimized for and Compatible to Vertical Field Open MRI. In: International Conference on Medical Image Computing and Computer-Assisted Intervention—MICCAI 2002 Lect Notes Comput Sci; Springer, Berlin, Heidelberg. 2002, pp. 114-121.
- Groenhuis V, Siepel FJ, Veltman J, van Zandwijk JK, Stramigioli S, Stormram 4: an MR safe robotic system for breast biopsy. *Ann Biomed Eng*. 2018;46(10):1686-1696. <https://doi.org/10.1007/s10439-018-2051-5>
- Price KD, Sin VW, Mougnot C, et al. Design and validation of an MR-conditional robot for transcranial focused ultrasound surgery in infants. *Med Phys*. 2016;43(9):4983-4995. <https://doi.org/10.1118/1.4955174>
- Yiallouras C, Mylonas N, Damianou C. MRI-compatible positioning device for guiding a focused ultrasound system for transrectal treatment of prostate cancer. *Int J Comput Assist Radiol Surg*. 2014;9(4):745-753. <https://doi.org/10.1007/s11548-013-0964-x>
- Yiallouras C, Ioannides K, Dadakova T, Pavlina M, Bock M, Damianou C. Three-axis MR-conditional robot for high-intensity focused ultrasound for treating prostate diseases transrectally. *J Ther Ultrasound*. 2015;3(1):1-10. <https://doi.org/10.1186/s40349-014-0023-2>
- Patel NA, Nycz CJ, Carvalho PA, et al. An integrated robotic system for MRI-guided neuroablation: preclinical evaluation. *IEEE Trans Biomed Eng*. 2020;67(10):2990-2999.
- Krieger A, Song S-E, Cho NB, et al. Development and evaluation of an actuated MRI-compatible robotic system for MRI-guided prostate intervention. *IEEE ASME Trans Mechatron*. 2013;18(1):273-284. <https://doi.org/10.1109/TMECH.2011.2163523>
- Moreau-gaudry JGA, Hungr N, Moreau-gaudry A, et al. Evaluation of the needle positioning accuracy of a light puncture robot under MRI guidance: results of a clinical trial on healthy volunteers. *Cardiovasc Intervent Radiol*. 2018;41(9):1428-1435. <https://doi.org/10.1007/s00270-018-2001-5>
- Yiallouras C, Damianou C. Review of MRI positioning devices for guiding focused ultrasound systems. *Int J Med Robot Comput Assist Surg*. 2015;11:247-255. <https://doi.org/10.1002/rcs.1601>



16. Wu T. A quality control program for MR-guided focused ultrasound ablation therapy. *J Appl Clin Med Phys*. 2002;3(2):162. <https://doi.org/10.1120/1.1459262>
17. Mylonas N, Damianou C. MR compatible positioning device for guiding a focused ultrasound system for the treatment of brain diseases. *Int J Med Robot Comput Assist Surg*. 2014;10:1-10.
18. Sagias G, Yiallouras C, Ioannides K, Damianou C. An MRI-conditional motion phantom for the evaluation of high-intensity focused ultrasound protocols. *Int J Med Robot Comput Assist Surg*. 2016;12:431-441.
19. An CY, Syu JH, Tseng CS, Chang CJ. An ultrasound imaging-guided robotic HIFU ablation experimental system and accuracy evaluations. *Appl Bionics Biomech*. 2017;2017:1-8. <https://doi.org/10.1155/2017/5868695>
20. Menikou G, Damianou C. Acoustic and thermal characterization of agar based phantoms used for evaluating focused ultrasound exposures. *J Ther Ultrasound*. 2017;5:1-14. <https://doi.org/10.1186/s40349-017-0093-z>
21. Damianou C, Ioannides K, Milonas N. Positioning device for MRI-guided high intensity focused ultrasound system. *Int J Comput Assist Radiol Surg*. 2008;2(6):335-345. <https://doi.org/10.1007/s11548-007-0145-x>
22. Epaminonda E, Drakos T, Kalogirou C, Theodoulou M, Yiallouras C, Damianou C. MRI guided focused ultrasound robotic system for the treatment of gynaecological tumors. *Int J Med Robot Comput Assist Surg*. 2016;12:46-52.
23. Yiannakou M, Menikou G, Yiallouras C, Ioannides C, Damianou C. MRI guided focused ultrasound robotic system for animal experiments. *Int J Med Robot Comput Assist Surg*. 2017;13(4):e1804. <https://doi.org/10.1002/rcs.1804>

**How to cite this article:** Antoniou A, Drakos T, Giannakou M, et al. Simple methods to test the accuracy of MRgFUS robotic systems. *Int J Med Robot*. 2021;17(4):e2287. <https://doi.org/10.1002/rcs.2287>